Published in final edited form as:

Nature. ; 533(7604): 557–560. doi:10.1038/nature17636.

Structural insights into inhibition of Lipid I production in bacterial cell wall synthesis

Ben C. Chung[#1], **Ellene H. Mashalidis**[#1], **Tetsuya Tanino**[2], **Mijung Kim**[3], **Akira Matsuda**[2], **Jiyong Hong**[3], **Satoshi Ichikawa**[2], and **Seok-Yong Lee**[1,†]

[1] Department of Biochemistry, Duke University Medical Center, 303 Research Drive, Durham, North Carolina, 27710, USA

[2] Faculty of Pharmaceutical Sciences, Hokkaido University, Kita-12, Nihi-6, Kita-ku, Sapporo 060-0812, Japan

[3] Department of Chemistry, Duke University, Durham, North Carolina, 27708, USA

[#] These authors contributed equally to this work.

Summary

Antibiotic-resistant bacterial infection is a serious threat to public health. Peptidoglycan biosynthesis is a well-established target for antibiotic development. MraY (phospho-MurNAc-pentapeptide translocase) catalyzes the first and an essential membrane step of peptidoglycan biosynthesis. It is considered a very promising target for the development of new antibiotics, as many naturally occuring nucleoside inhibitors with antibacterial activity target this enzyme[1-4]. However, antibiotics targeting MraY have not been developed for clinical use mainly due to a lack of structural insight into inhibition of this enzyme. Here we present the crystal structure of MraY from *Aquifex aeolicus* ($MraY_{AA}$) in complex with its naturally occurring inhibitor, muraymycin D2 (MD2). Upon binding MD2, $MraY_{AA}$ undergoes remarkably large conformational rearrangements near the active site, which lead to the formation of a nucleoside-binding pocket and a peptide-binding site. MD2 binds the nucleoside-binding pocket like a two-pronged plug inserting into a socket. Additional interactions it makes in the adjacent peptide-binding site anchor MD2 to and enhance its affinity for $MraY_{AA}$. Surprisingly, MD2 does not interact with three acidic residues or the Mg^{2+} cofactor required for catalysis, suggesting that MD2 binds to $MraY_{AA}$ in a manner that overlaps with, but is distinct from its natural substrate, UDP-MurNAc-pentapeptide. We have deciphered the chemical logic of MD2 binding to $MraY_{AA}$, including how it avoids the need for pyrophosphate and sugar moieties, which are essential features for substrate

[†]Correspondence to: S.-Y. Lee. seok-yong.lee@duke.edu, tel: 919-684-1005, fax: 919-684-8885.

Author Contributions B.C. solved the structures and performed some of ITC experiments and E.M. carried out the enzymatic assays and performed most of ITC experiments, both under the guidance of S.-Y.L. T.T. carried out chemical synthesis of MD2 under the guidance of S.I. and A.M. M.K. synthesized 5-aminoribosyl-3-deoxyuridine under the guidance of J.H. S.-Y.L., E.M., and B.C. wrote the paper. All authors discussed the results and commented on the manuscript.

Atomic coordinates and structure factors for the reported crystal structure are deposited in the Protein Data Bank under accession code 5CKR. The authors declare no competing financial interests.

A **supplementary video** is included in a separate file.

binding. The conformational plasticity of MraY could be the reason that it is the target of many structurally distinct inhibitors. These findings can inform the design of new inhibitors targeting MraY as well as its paralogs, WecA and TarO.

MraY is a member of the polyprenylphosphate *N*-acetyl hexosamine 1-phosphate transferase (PNPT) superfamily. The PNPT superfamily includes bacterial and eukaryotic integral membrane enzyme families such as MraY, WecA, TarO, WbcO, WbpL, RgpG, and GPT, which are involved in cell envelope polymer synthesis and protein N-linked glycosylation [1]. WecA and TarO are also targets for antibiotic development. MraY catalyzes the transfer of phospho-MurNAc-pentapeptide from UDP-MurNAc-pentapeptide (UM5A) to the lipid carrier undecaprenyl phosphate (C_{55}-P), yielding undecaprenyl-pyrophosphoryl-MurNAc-pentapeptide, known as Lipid I (Extended Data Fig. 1a). This step is essential, rate limiting, and Mg^{2+}-dependent [1]. It is blocked by five classes of natural nucleoside antibiotics (e.g. muraymycin and tunicamycin), and bacteriolytic protein E from bacteriophage phiX174, with various modes of inhibition (Extended Data Fig. 1a) [5-8]. MraY-targeted natural products have gained attention because of their *in vivo* efficacy against pathogenic bacteria including *M. tuberculosis,* methicillin-resistant *S. aureus* (MRSA), and vancomycin-resistant *Enterococcus* (VRE) [6,9-12]. Despite their promise, no antibacterial natural products that target MraY have been developed for clinical use, in part due to a lack of structural information on MraY catalysis and inhibition. We carried out structural studies of MraY in complex with a naturally occurring inhibitor of MraY, muraymycin, which shows antibacterial effects against MRSA, VRE, and *P. aeuruginosa,* and *S. aureus* [11,13-18]. We used muraymycin D2 (MD2) for our structural, enzymatic, and biophysical studies (Extended Data Fig. 1b) [17]. The muraymycins are known to be competitive inhibitors for the natural substrate UM5A [14]. Unlike UM5A, the muraymycins do not have pyrophosphate and sugar moieties and have a 5-amino ribosyl group (Extended Data Fig. 1b). Using a radiochemical transfer assay [19], we determined the K_M for UM5A with purified $MraY_{AA}$ to be ~190 μM (Extended Data Fig 1c), which is within the range of measured cellular UM5A concentrations [20]. $MraY_{AA}$ activity is significantly reduced upon addition of 0.3 μM MD2 (Fig. 1a). Using isothermal titration calorimetry (ITC), we measured the K_D of MD2 for $MraY_{AA}$ to be ~20 nM (Fig. 1b). We generated crystals of $MraY_{AA}$ in the presence of MD2, which diffracted to 2.95 Å. Phasing was obtained by molecular replacement (MR) using the apo$MraY_{AA}$ structure (PDB ID: 4J72) with all the cytoplasmic loops and TM9b removed as a search model. The structure was refined to good statistics (R/R_{free} = 0.247/0.261) (Extended Data Table 1).

$MraY_{AA}$ in complex with MD2 crystallizes as a dimer, as does apo$MraY_{AA}$ [21]. Each protomer contains ten transmembrane helices (TM1-TM10) and five cytoplasmic loops (loops A-E) (Fig. 2a). TM9 breaks into two helical fragments (TM9a and TM9b) and TM9b bends outward toward the membrane (Fig. 2b). We previously outlined the active site as a cleft formed by the inner-leaflet membrane regions of TMs 3, 4, 5, 8, and 9b and cytoplasmic loops B, C, D, and E. Many absolutely conserved polar/charged amino acid residues are localized in this cleft, including three catalytically critical acidic residues: Asp117, Asp118, and Asp265 (Fig. 2a and 2c), which are conserved in the PNPT superfamily [1,19,21-23]. Asp265 interacts with Mg^{2+} in the apo$MraY_{AA}$ structure and Asp117

has been proposed to bind to the phophate moiety of C_{55}-P [21,22]. Situated in the active site cleft, the nucleoside portion of MD2 is inserted between loop C and loop D and the peptide portion interacts with TM9b and loop E (Fig. 2c). High sequence conservation is observed around the MD2-binding region in the active site (Fig. 2d). Interestingly, MD2 does not interact with any of the three catalytically critical acidic residues (Fig. 2c and Extended Data Fig. 1d). MraY undergoes remarkable conformational rearrangements near the active site upon binding MD2 (Fig. 3). The amphipathic TM9b rotates away from the active site while loop E rearranges, packs against the hydrophilic part of TM9b (Extended Data Fig. 2 and Supplementary video), and a helical segment of the conserved HHH motif (PXHHHXEXXG) extends [1,21]. This TM9b-loop E rearrangement widens and reshapes the active site, allowing the peptidic moiety of MD2 to bind to the side of TM9b and loop E (Extended Data Fig 3). The C-terminal portion of TM5 and loop C unwinds (cyan, Fig 3, a-b) and loop D rearranges (magenta, Fig 3, a-b), creating a pocket where the 5-aminoribosyl moiety and the uracil base of uridine interact (Fig. 3d and Extended Data Fig. 4a-c). The concerted motions of TM5 and loops C and D lead to the rearrangement of loop A and part of TM1 (green, Fig. 3b), although these regions do not appear to interact with MD2 directly. It is noteworthy that the amino acid residues interacting with the uracil base move large distances (5-17 Å) while the residues interacting with the 5-aminoribosyl moiety move shorter distances (Extended Data Fig. 4a-c and Supplementary video). The active-site structural rearrangement leads to substantial changes in its electrostatic potential, including enlargement of the acidic milieu around the nucleoside-binding pocket, which may play a role in MD2 binding (Fig. 3, c-d).

Developing nucleotide-sugar mimicking inhibitors for glycosyltransferases has been challenging largely due to the difficulty of developing pyrophosphate mimics capable of cellular entry with high affinity for the target enzyme [24-27]. MraY is a phosphoglycosyltransferase that shares a common nucleotide sugar substrate with glycosyltransferases. Nucleoside antibiotics targeting MraY have garnered interest because they can enter the cell with high affinity for MraY [24,25,28]. MD2 does not contain a pyrophosphate or sugar moiety and has a 5-amino ribosyl group, which was thought to mimic the pyrophosphate in the natural substrate UM5A (Extended Data Fig. 1b) [23,29]. To understand the principle of MD2 inhibition of $MraY_{AA}$, we performed mutagenesis and measured the mutational effects on MD2 binding using ITC. Amino acid residues involved in binding MD2 were grouped based on the substructures with which they interact: 1) uracil (Lys70, Gly194, Asp196, Asn255, and Phe262), 2) 5-amino ribose (Thr75, Asn190, Asp193, and Gly264), and 3) peptidic sidechain (Gln305, Ala321, and His325). We performed site-directed mutagenesis on the residues that form side-chain interactions with MD2 (Lys70, Thr75, Asn190, Asp193, Asp196, Asn255, Phe262, Gln305, His325) (Fig. 4). The $MraY_{AA}$ mutants that showed significant enzyme activity (Extended Data Fig. 5) were used for ITC experiments with MD2 (Extended Data Fig. 6 and Extended Data Table 2).

The affinity of MD2 for $MraY_{AA}$ was most perturbed with D193N and F262A, mutations that disrupt interactions with the 5-aminoribose and uracil moieties of MD2, respectively (Fig. 4, Extended Data Table 2, and Extended Data Fig. 6). Phe262 interacts with the uracil base via a π-π interaction (Fig. 4 and Extended Data Fig. 4d). When Phe262 is mutated to another aromatic amino acid, such as tryptophan, there is a smaller effect on K_D relative to

the alanine mutation, indicating the importance of this π-π interaction. Residue Asp193 makes sidechain interactions with the 5-amino ribose moiety of MD2 (Extended Data Fig. 4e). Because the D193A mutant is nearly inactive (Extended Data Fig. 5b), we used functionally competent D193N for ITC with MD2 (Extended Data Fig. 5a). However, the heat associated with binding was too low to measure, suggesting the D193N mutation greatly reduces the affinity of MD2 for $MraY_{AA}$ (Extended Data Fig. 6). This observation is consistent with previous studies indicating the antibacterial activity of MraY inhibitors with a 5-aminoribose is dependent on the amino group of that moiety [29,30]. The Q305A mutant exhibits a larger than five-fold increase in K_D (Fig. 4 and Extended Data Table 2), indicating that the interactions formed by the peptidic moiety of MD2 contribute to the binding affinity. Asp193, Phe262, and Gln305 are absolutely conserved in MraY orthologs [21]. The results from the equilibrium binding experiments are consistent with the enzymatic inhibition experiments because the F262A mutation results in partial inhibition and the D193N mutant is not inhibited in the presence of 1 μM MD2 (Extended Data Fig. 5a).

We infer that MD2 and the natural substrate, UM5A, utilize different strategies for binding MraY. First, the three catalytically critical acidic residues, including the Mg^{2+}-binding Asp265, do not participate in direct interactions with MD2 (Extended Data Fig. 1d). Second, the D193N mutant remains functionally active, although it disrupts an interaction MraY makes with the 5-aminoribosyl group and affects the binding affinity of MD2 dramatically (Extended Data Table 2 and Extended Data Fig. 6). This suggests the 5-aminoribosyl group does not function as a pyrophosphate mimic and instead forms interactions that are not present in or important for UM5A binding. If MD2 lacks a pyrophosphate mimic, it is unlikely that Mg^{2+} plays an important role in MD2 binding. To test this idea, we performed ITC in the absence of Mg^{2+} and found that MD2 does not require Mg^{2+} for MraY binding (Fig. 4c). It is possible that the amino group of the 5-aminoribose mimics Mg^{2+} and Asp193 interacts with Mg^{2+}, as previously suggested [14]. However, in such a case, we would expect D193N to be inactive. Furthermore, the amino group of the 5-aminoribose is not near the Asp265, which coordinates Mg^{2+} in the apoMraY structure [21].

In summary, the 5-aminoribosyl and uracil moieties of MD2 bind to the nucleoside-binding pocket like a two-pronged electrical plug inserts into a socket, and these interactions are the most critical for binding. The peptidic moiety also contributes to the binding energy by anchoring MD2 to MraY, likely contributing to its specificity for MraY. With the 5-aminoribose moiety of MD2 positioned as a second prong alongside uridine in the nucleoside binding site, MD2 binds to MraY with increased affinity, making the pyrophosphate and sugar moieties unnecessary for binding. To confirm the importance of the 5-aminoribosyl and uracil moieties of MD2, we synthesized 5-aminoribosyl-3-deoxy uridine [29] and found it retains substantial binding affinity for $MraY_{AA}$ (Fig 4d). Our structural and biochemical studies demonstrate the principles of MD2 inhibition of MraY and explain why MD2 does not require pyrophosphate and sugar moieties for binding, unlike the natural substrate, UM5A. This illustrates an example of nature circumventing a long-standing problem in chemical biology: developing a nucleotide-sugar-like inhibitor for glycosyltransferases [24-27]. Finally, the large conformational arrangement observed in MraY implies conformational plasticity, which could be the reason why MraY accommodates so

many structurally different nucleoside inhibitors, as well as protein E, with distinct modes of action [7].

Methods

Crystallization

Wild-type $MraY_{AA}$ and mutants were expressed and purified as described [21]. All $MraY_{AA}$ bacterial expression plasmids were 10x histidine (His_{10})-maltose binding protein (MBP) fusion constructs expressed in C41 (DE3) cells. The cells were lysed by microfluidizer and the protein was extracted from the crude lysate using 40 mM dodecyl-maltoside. The lysates were centrifuged to remove the insoluble fraction and the supernatant was applied to a Co^{2+}-affinity column for purification. The His_{10}-MBP tag was cleaved overnight by PreScission Protease and $MraY_{AA}$ was isolated by gel filtration using a Superdex 200 10/300 GL column in the presence of 5 mM decyl-maltoside, 150mM NaCl, 20mM Tris-HCl pH 8.0, and 2mM DTT. All purification steps were performed at 4 °C. After gel filtration, the protein was concentrated to ~10 mg/ml (~250 μM) and MD2 was added to a final concentration of 400-500 μM before crystallization. Crystals were grown using sitting-drop vapor diffusion in the presence of 50 mM $MgCl_2$, 40% PEG400, and 100 mM sodium cacodylate pH 5.6. Crystals were harvested after 10–14 days and flash frozen in liquid nitrogen.

Data Collection and Structure Determination

X-ray data were collected at beamlines 22-ID-D and 24-ID-C at the Advanced Photon Source in Argonne National Laboratory at a wavelength of 1.0 Å and processed using iMosflm. The data were ellipsoidally truncated at 3.0 Å on the *c* axis and anisotropically scaled using the UCLA anisotropy diffraction server (http://services.mbi.ucla.edu/anisoscale/). Phases of the MD2 complex structures were solved by molecular replacement using PHASER [31] with a partial apo$MraY_{AA}$ structure (PDB ID: 4J72, TM9b and cytoplasmic loops removed) as the search model. The omit electron density peaks corresponding to MD2 were prominent from the beginning of the refinement. After the protein model was built, a simulated annealing omit map was generated and MD2 was modeled. PHENIX [32] and Coot [33] were used to refine the structure. The final model has good geometry with 98.8%/1.2%/0.0% Ramachandran favored/allowed/outliers.

Enzymatic Assays

All enzymatic assays monitored the $MraY_{AA}$-mediated transfer of [^{14}C]phospho-MurNAc-pentapeptide from [^{14}C]UDP-MurNAc-pentapeptide(DAP) ([^{14}C]UM5A) to undecaprenyl phosphate (C_{55}-P), forming [^{14}C]Lipid I. A radiochemical transfer assay [19] was used, which was optimized for the $MraY_{AA}$-catalyzed reaction as follows. Reaction mixtures (20 μL each) containing 100 mM Tris-HCl pH 8.0, 500 mM NaCl, 10 mM $MgCl_2$, 20 mM CHAPS, and 250 μM C_{55}-P were incubated at 45 °C for 5-6 min in the presence of 0 μM, 0.3 μM, or 1.0 μM MD2. For the specific activity assays, 150 μM [^{14}C]UM5A (3.6 nCi/assay) was used. For $MraY_{AA}$ WT K_M and k_{cat} determination, [^{14}C]UM5A concentration varied from 25 μM to 750 μM (0.6 – 17.9 nCi/assay). The substrate [^{14}C]UM5A (specific radioactivity: 1.19×10^{-3} Ci/mmol) was purchased from the BaCWAN facility at the University of Warwick [34]. $MraY_{AA}$ WT or mutant $MraY_{AA}$ was added to the reaction mixture to a final

concentration that enabled product detection within the enzymatic linear range: 50 nM (WT), 500 nM (K70A), 400 nM (T75A), 350 nM (D193N), 250 nM (N255A), 200 nM (F262A), 50 nM (F262W), 400 nM (Q305A), and 500 nM (H325A). The mutant $MraY_{AA}$ enzymes N190A, D193A, and D196A were added to the reaction mixture at a final concentration of 500 nM. All WT and mutant $MraY_{AA}$ enzymes were purified as previously described [21]. Each reaction was initiated with the addition of enzyme and it was quenched with 20 μL of 6 M pyridinium acetate, pH 3.0. The radiolabeled product, [^{14}C]Lipid I, was isolated from the hydrophilic substrate, [^{14}C]UM5A, with butanol extraction (200 μL). After vortexing (30 s) and centrifugation at 3000 ×g (5 min), the upper butanol phase was removed, added to 5 mL scintillation fluid (Fisher Chemical), and analyzed using a liquid scintillation counting method (dpm) for ^{14}C detection (Packard 2500 TR Liquid Scintillation Analyzer). Control reactions lacking enzyme and inhibitor were incubated, extracted, and analyzed following same protocol described above and were used for background subtraction. Each reaction rate was calculated by converting the dpm measured (with background subtraction) to moles of [^{14}C]-Lipid I formed using the specific radioactivity and dividing by the reaction time. All experiments were performed in triplicate (technical replicates).

Chemical Synthesis

Muraymycin D2 (MD2) was synthesized as published [17]. The MD2 analog, 5-aminoribosyl 3-deoxyuridine, was synthesized as published [35], with a minor modification as follows. In the coupling of the hexose with the ribose, we replaced 5-azido-5-deoxy-D-ribofuranosyl chloride 2, 3-diacetate in the original procedure with a synthetically equivalent 5-azido-5-deoxy-2,3-*O*-(1-methylethylidene)-D-ribofuranosyl fluoride since the ribofuranosyl fluoride was previously prepared in our laboratory [36]. Except for this minor modification, our synthesis of the MD2 analog was identical to the original synthesis by Dini *et al* [35].

Isothermal Titration Calorimetry

$MraY_{AA}$ WT and mutants (K70A, T75A, D193N, N255A, F262A, F262W, Q305A, and H325A) were purified as previously described [21] in a buffer containing 150mM NaCl, 20mM Tris-HCl pH 8.0, 4 mM DM, 2mM DTT and 10 mM $MgCl_2$. This same buffer was used to dilute the ligand, MD2. One triplicate set of titrations with $MraY_{AA}$ WT and MD2 did not include $MgCl_2$. For $MraY_{AA}$ WT, 145-240 μM MD2 or 118-130 μM 5-aminoribosyl-3-deoxy uridine was titrated into 6.6-35 μM enzyme. For $MraY_{AA}$ mutants K70A, T75A, D193N, N255A, F262W, and H325A, 210 μM MD2 was titrated into 30 μM enzyme. For $MraY_{AA}$ Q305A, 315-430 μM MD2 was titrated into 25-27 μM enzyme. For $MraY_{AA}$ F262A, 80-110 μM MD2 was titrated into 7-10.5 μM enzyme. All titrations were performed in triplicate (technical replicates) at 37°C using either a MicroCal iTC200 or VP-ITC system (GE Healthcare). The total heat exchanged during each injection was fit to a single-site binding isotherm with K^D and ΔH° as independent parameters. Data were analyzed and figures were generated using Origin software (OriginLab Corp).

Extended Data

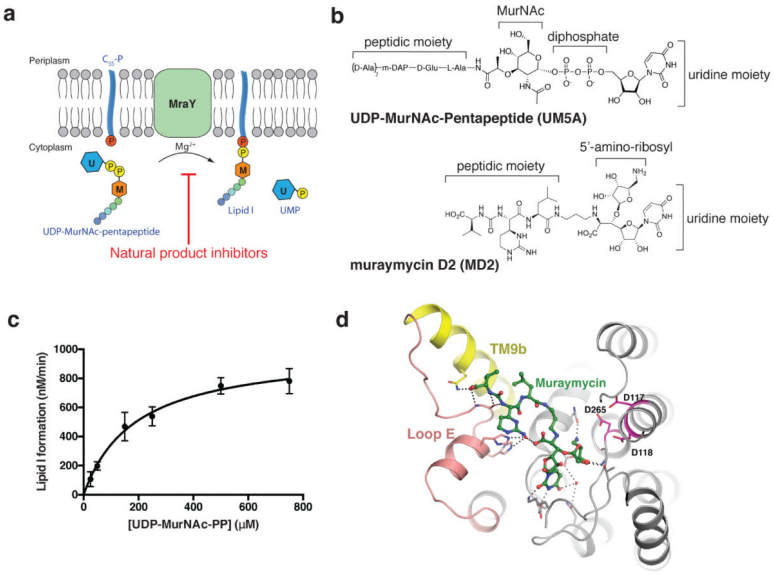

Extended Figure 1.

MraY catalyzes the formation of Lipid I and binds MD2. a, Scheme of the reaction catalyzed by MraY. The U-labeled blue hexagon represents uridine and the M-labeled orange hexagon represents MurNAc. The phosphates associated with the lipid carrier C_{55}-P are shown as red circles, and the phosphates from the substrate, UDP-MurNAc-pentapeptide (UM5A), are shown as yellow circles. **b**, Chemical structures of the substrate, UM5A (top) and the inhibitor MD2 (bottom). **c**, Michaelis-Menten kinetic characterization of $MraY_{AA}$ translocase activity. The reaction monitored is the $MraY_{AA}$-catalyzed transfer of [^{14}C]phospho-MurNAc-pentapeptide from [^{14}C]UM5A to C_{55}-P, forming [^{14}C]Lipid I. The enzymatic parameters measured are as follows: K_M = 190 ± 60 μM, k_{cat} = 20 ± 2 min^{-1}, k_{cat}/K_M = 0.11 ± 0.3 μM^{-1} min^{-1}. Data are shown as means of three technical replicates ± s.e.m. **d**, MD2 (green) in complex with $MraY_{AA}$. The distances between MD2 and the three catalytic acidic residues D117, D118 and D265 (magenta) are all greater than 4.5 Å.

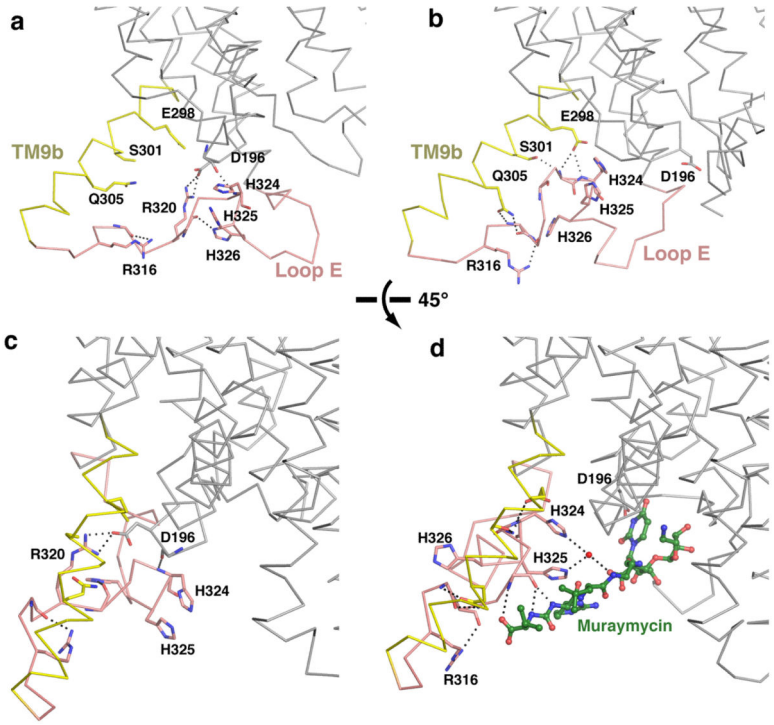

Extended Figure 2.

Conformational changes of the TM9b and loop E region of $MraY_{AA}$ upon MD2 binding. a, Zoomed-in view of TM9b (yellow) and loop E (pink) of apo$MraY_{AA}$, viewed from within the membrane. **b,** TM9b and loop E of MD2-bound $MraY_{AA}$ viewed from within the membrane. MD2 is omitted to illustrate the conformational change of TM9b and loop E associated with MD2 binding. Conserved amino acid residues and their interactions are shown in stick representation as dotted lines, respectively. **c,** 45-degree rotated view of (**a**) about a horizontal axis. **d,** 45-degree rotated view of (**b**) about a horizontal axis, including the model of MD2 (green). The rotation of TM9b and rearrangement of loop E, including the HHH motif, allows for MD2 binding, especially its peptidic moiety.

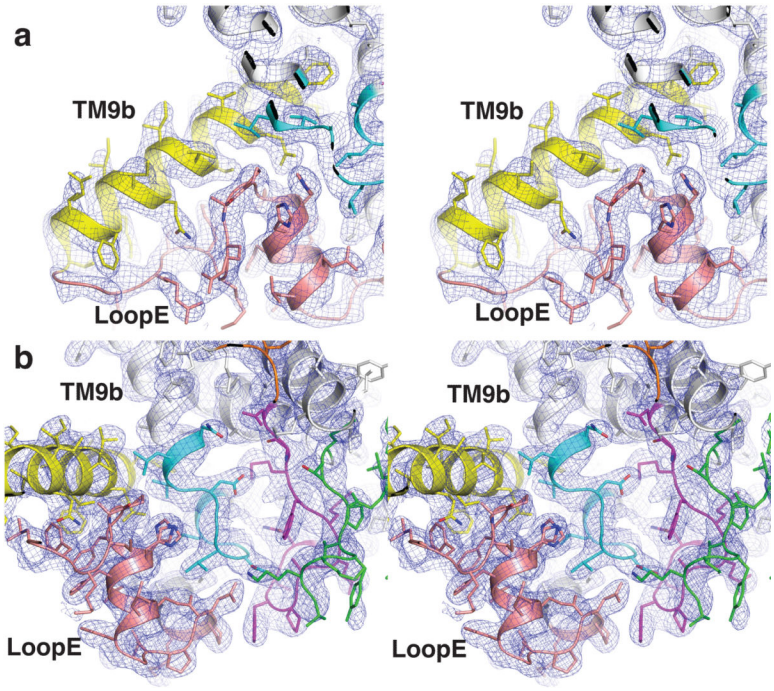

Extended Figure 3.

Quality of electron density map surrounding MD2. a, Stereo view of $2F_o–F_c$ electron density map at 1σ for TM9b and loop E. **b.** Stereo view of $2F_o–F_c$ electron density map at 1σ for the MD2 binding pocket. The electron density peaks corresponding to MD2 are carved for clarity and all TMs are colored as in Fig. 3.

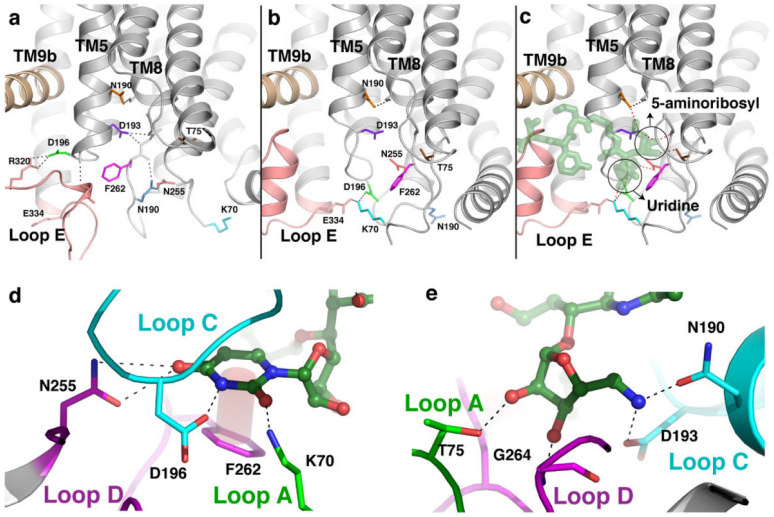

Extended Figure 4.

Conformational changes in $MraY_{AA}$ that create binding pockets for the uridine and 5-amino ribosyl groups of MD2. a, A close-up view of apo$MraY_{AA}$ with key residues that participate in conformational changes upon MD2 binding shown as sticks in various colors. **b,** A close-up view of the nucleoside-binding pocket in the $MraY_{AA}$-MD2 complex with MD2 omitted. Key residues are colored as in **(a)**. **c,** A close-up view of the interactions MD2 (green) makes

with the nucleoside-binding pocket of $MraY_{AA}$. Interactions between $MraY_{AA}$ and MD2 are shown as dotted lines. It is noteworthy that residues interacting with the uridine moiety of MD2 move large distances (5-17 Å for residues K70, D196, N255, and F262), while the residues binding the 5-aminoribosyl group of MD2 (T75, N190, and D193) do not make large sidechain movements upon MD2 binding. The uridine and 5-amino ribosyl groups of MD2 are circled. **d,** Interactions between the uracil base of MD2 (green) and the nucleoside-binding pocket of $MraY_{AA}$. The uracil base forms H-bonds with side chains of N255, D196 and K70 and forms a π - π interaction with F262. **d**, The 5-amino ribosyl group of MD2 forms H-bond interactions with side chains of T75, N190, and D193, and the backbone amide of G264.

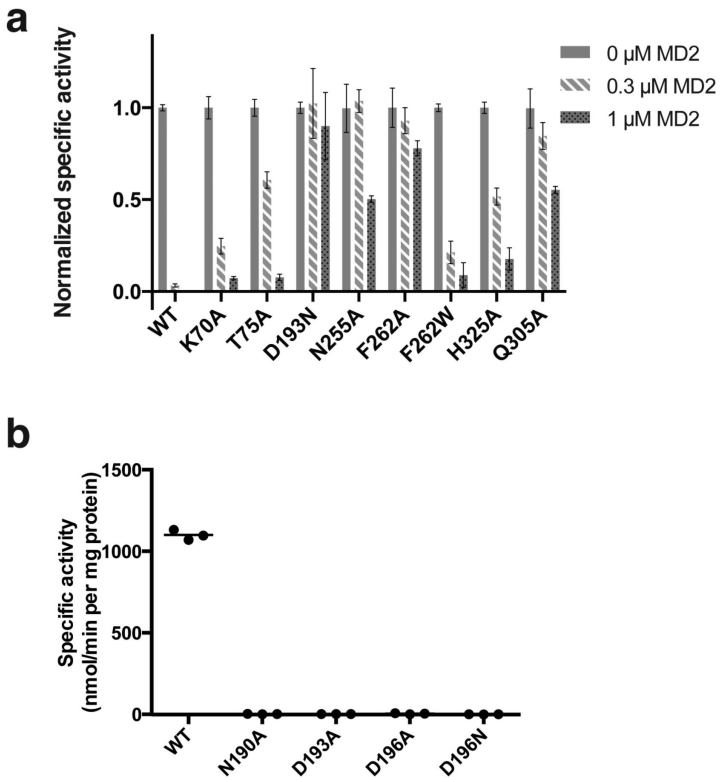

Extended Figure 5.

Specific activity of $MraY_{AA}$ WT and mutants in the presence and absence of MD2. a, Normalized specific activity of $MraY_{AA}$ WT and enzymatically active mutants with and without MD2 treatment. $MraY_{AA}$ WT or mutant $MraY_{AA}$ was added to the reaction mixture to a final concentration that enabled product detection within the enzymatic linear range: 50 nM (WT), 500 nM (K70A), 400 nM (T75A), 350 nM (D193N), 250 nM (N255A), 200 nM (F262A), 50 nM (F262W), 400 nM (Q305A), and 500 nM (H325A). Each reaction was carried out in the presence of either 0 μM, 0.3 μM, or 1 μM MD2. Data are shown for three technical replicates ± s.e.m. Specific activity measurements for each mutant were normalized relative to that without added MD2. **b,** Specific activity of $MraY_{AA}$ WT and enzymatically inactive mutants. $MraY_{AA}$ N190A, D193A, D196A, and D196N were each added to a final concentration of 500 nM, while $MraY_{AA}$ WT was present at 50 nM. All enzymatic reactions were conducted with a radiochemical assay monitoring the transfer of

[^{14}C]phospho-MurNAc-pentapeptide from [^{14}C]UM5A to C_{55}-P, forming [^{14}C]Lipid I. The radiolabeled product, [^{14}C]Lipid I, was quantified using a liquid scintillation counting method (dpm). Specific activity was calculated by determining moles of [^{14}C]-Lipid I formed, divided by the reaction time and the quantity of enzyme added. Three technical replicates are shown with the mean value indicated by a line.

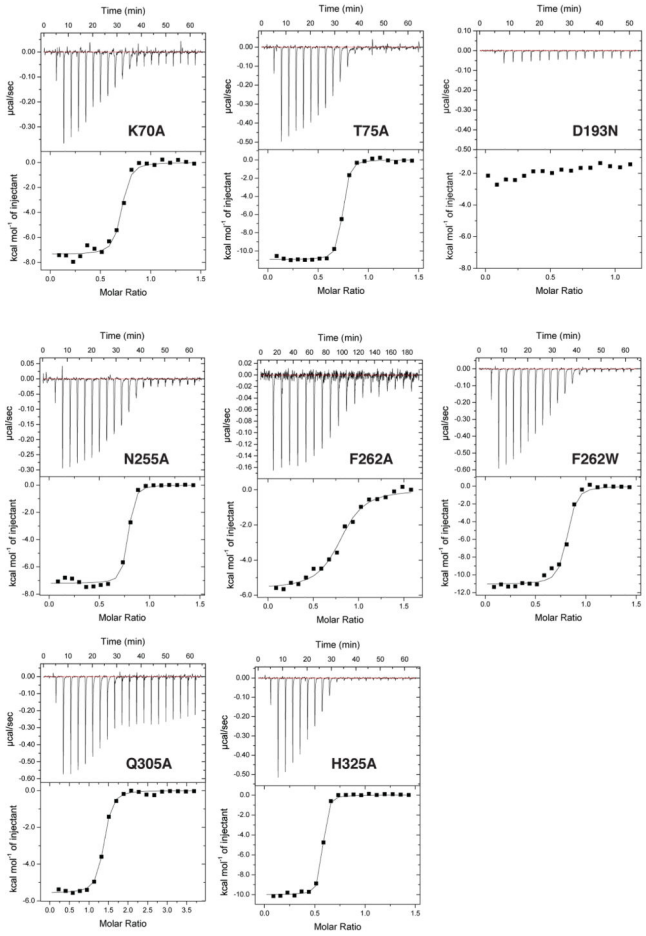

Extended Figure 6.

Representative ITC raw data and binding isotherms for MD2 interacting with mutant MraY$_{AA}$. All titrations were performed in triplicate (technical replicates); see source data for all titrations. Representative data is shown. For MraY$_{AA}$ mutants K70A, T75A, D193N, N255A, F262W, and H325A, 210 µM MD2 was titrated into 30 µM enzyme. For MraY$_{AA}$ Q305A, 315-430 µM MD2 was titrated into 25-27 µM enzyme. For MraY$_{AA}$ F262A, 80-110 µM MD2 was titrated into 7-10.5 µM enzyme. Mean thermodynamic parameters for triplicate titrations are shown in the Extended Data Table 2. Mean K_D values for each triplicate are as follows: 63.9 ± 4.7 nM for K70A; 27.4 ± 1.5 nM for T75A; K_D not determined for D193N; 29.7 ± 0.8 nM for N255A; 228 ± 4 nM for F262A; 68.4 ± 0.9 nM for F262W; 117 ± 10 nM for Q305A; 24.4 ± 0.4 nM for H325A.

Extended Data Table 1

Data collection and refinement statistics

$MraY_{AA}$-Muraymycin D2	
Data collection	
Space group	C 2 2 2_1
Cell dimensions	
a, *b*, *c* (Å)	94.48, 102.05, 135.8
α, β, γ (°)	90, 90, 90
Resolution (Å)	2.95 (3.06 – 2.95)*
R_{merge} (%)	27.7 (>100)
R_{pim} (%)	11.6 (64.5)
$I/\sigma I$	4.6 (1.2)
$CC_{1/2}$ (%)	87.4 (50.2)
Completeness (%)	100 (100)
Redundancy	7.0 (6.3)
Refinement	
Resolution (Å)	2.95 (3.18 – 2.95)†
No. reflections	14053
Completeness (%)	99.40 (93.90)
R_{work} / R_{free}(%)	24.7/26.1
No. atoms	
Protein	2576
Ligand/ion	64
Water	9
B-factors	
Protein	63.50
Ligand/ion	60.50
Water	50.00
R.m.s. deviations	
Bond lengths (Å)	0.008
Bond angles (°)	1.14
Molprobity	
Overall	1.75
Ramachandran (%)	
Favored	99 1
Allow	0.9
Outlier	0

*Values in parentheses are for highest-resolution shell.

†Anisotropic truncation at 3.0 Å on *c* axis by the UCLA Diffraction Anisotropy Server http://services.mbi.ucla.edu/anisoscale/

Extended Data Table 2

Equilibrium dissociation constants (K_Ds) and binding parameters demonstrating the effect of mutation in $MraY_{AA}$ on MD2 binding.

	K_D (nM)	N (sites)	ΔH (kcal/mol)	ΔS (cal/mol/deg)
WT +Mg^{2+}	20.4 ± 1.9	0.62 ± 0.02	−15.0 ± 3.5	−11.5 ± 9.8
WT −Mg^{2+}	15.1 ± 0.2	0.65 ± 0.05	−9.1 ± 0.6	6.5 ± 2.0
K70A	63.9 ± 4.7	0.72 ± 0.05	−7.2 ± 0.2	9.8 ± 0.7
T75A	27.4 ± 1.5	0.71 ± 0.01	−11.7 ± 0.6	−3.3 ± 1.7
D193N	-	-	-	-
N255A	29.7 ± 0.8	0.68 ± 0.06	−7.6 ± 0.3	10.1 ± 1.1
F262A	228 ± 4	0.77 ± 0.07	−4.9 ± 0.8	14.7 ± 2.5
F262W	68.4 ± 0.9	0.81 ± 0.03	−10.4 ± 0.7	−0.7 ± 2.2
Q305A	117 ± 10	0.73 ± 0.08	−9.8 ± 0.3	0.1 ± 1.0
H325A	24.4 ± 0.4	0.56 ± 0.07	−11.3 ± 0.7	−1.7 ± 2.2
WT + 5-aminoribosyl-3-deoxy uridine	283 ± 3	0.44 ± 0.02	−15.0 ± 1.5	−19.9 ± 4.8

Data are shown as means of three technical replicates ± s.e.m.

Supplementary Material

Refer to Web version on PubMed Central for supplementary material.

Acknowledgements

Data for this study were collected at beamlines NE-CAT 24-ID-C and SER-CAT 22-ID-D and at the Advanced Photon Source. We thank K. Yokoyama for advice and guidance throughout the project and Z. Johnson for manuscript reading. Initial X-ray screening of crystals was performed at the Duke macromolecular crystallography facility. This work was supported by NIH R01 GM100984 (S.-Y.L.) and Duke startup funds (S.-Y.L.). This work was also supported by the JSPS Grant-in-Aid for Scientific Research on Innovative Areas “Chemical Biology of Natural Products” (S.I., Grant Number 24102502) and Scientific Research (B) (S.I., Grant Number 25293026).

References

1. Bouhss A, Trunkfield AE, Bugg TD, Mengin-Lecreulx D. The biosynthesis of peptidoglycan lipid-linked intermediates. FEMS Microbiol Rev. 2008; 32:208–233. doi:10.1111/j.1574-6976.2007.00089.x. [PubMed: 18081839]
2. Bugg TD, Lloyd AJ, Roper DI. Phospho-MurNAc-pentapeptide translocase (MraY) as a target for antibacterial agents and antibacterial proteins. Infect Disord Drug Targets. 2006; 6:85–106. [PubMed: 16789873]
3. Lecercle D, et al. Bacterial transferase MraY inhibitors: synthesis and biological evaluation. Bioorganic & medicinal chemistry. 2010; 18:4560–4569. doi:10.1016/j.bmc.2010.04.023. [PubMed: 20537545]
4. Shapiro AB, Jahic H, Gao N, Hajec L, Rivin O. A high-throughput, homogeneous, fluorescence resonance energy transfer-based assay for phospho-N- acetylmuramoyl-pentapeptide translocase (MraY). J Biomol Screen. 2012; 17:662–672. doi:10.1177/1087057112436885. [PubMed: 22337656]
5. Walsh CT, Zhang W. Chemical logic and enzymatic machinery for biological assembly of peptidyl nucleoside antibiotics. ACS chemical biology. 2011; 6:1000–1007. doi:10.1021/cb200284p. [PubMed: 21851099]
6. Winn M, Goss RJ, Kimura K, Bugg TD. Antimicrobial nucleoside antibiotics targeting cell wall assembly: recent advances in structure-function studies and nucleoside biosynthesis. Nat Prod Rep. 2010; 27:279–304. doi:10.1039/b816215h. [PubMed: 20111805]
7. Brandish PE, et al. Modes of action of tunicamycin, liposidomycin B, and mureidomycin A: inhibition of phospho-N-acetylmuramyl-pentapeptide translocase from Escherichia coli. Antimicrob Agents Chemother. 1996; 40:1640–1644. [PubMed: 8807054]
8. Bernhardt TG, Struck DK, Young R. The lysis protein E of phi X174 is a specific inhibitor of the MraY-catalyzed step in peptidoglycan synthesis. The Journal of biological chemistry. 2001; 276:6093–6097. doi:10.1074/jbc.M007638200. [PubMed: 11078734]
9. Bogatcheva E, et al. Chemical modification of capuramycins to enhance antibacterial activity. J Antimicrob Chemother. 2011; 66:578–587. doi:10.1093/jac/dkq495. [PubMed: 21186194]
10. Koga T, et al. Activity of capuramycin analogues against Mycobacterium tuberculosis, Mycobacterium avium and Mycobacterium intracellulare in vitro and in vivo. J Antimicrob Chemother. 2004; 54:755–760. doi:10.1093/jac/dkh417. [PubMed: 15347635]
11. McDonald LA, et al. Structures of the muraymycins, novel peptidoglycan biosynthesis inhibitors. J Am Chem Soc. 2002; 124:10260–10261. [PubMed: 12197711]
12. Nikonenko BV, et al. Activity of SQ641, a capuramycin analog, in a murine model of tuberculosis. Antimicrob Agents Chemother. 2009; 53:3138–3139. doi:10.1128/AAC.00366-09. [PubMed: 19414567]
13. Takeoka Y, et al. Expansion of Antibacterial Spectrum of Muraymycins toward Pseudomonas aeruginosa. ACS medicinal chemistry letters. 2014; 5:556–560. doi:10.1021/ml5000096. [PubMed: 24900879]

14. Tanino T, et al. Mechanistic analysis of muraymycin analogues: a guide to the design of MraY inhibitors. Journal of medicinal chemistry. 2011; 54:8421–8439. doi:10.1021/jm200906r. [PubMed: 22085339]
15. Tanino T, et al. Synthesis and Biological Evaluation of Muraymycin Analogues Active against Anti-Drug-Resistant Bacteria. ACS medicinal chemistry letters. 2010; 1:258–262. doi:10.1021/ml100057z. [PubMed: 24900205]
16. Tanino T, Ichikawa S, Matsuda A. Synthesis of L-epi-capreomycidine derivatives via C-H amination. Organic letters. 2011; 13:4028–4031. doi:10.1021/ol201527k. [PubMed: 21736287]
17. Tanino T, Ichikawa S, Shiro M, Matsuda A. Total synthesis of (−)-muraymycin D2 and its epimer. The Journal of organic chemistry. 2010; 75:1366–1377. doi:10.1021/jo9027193. [PubMed: 20143822]
18. Yamashita A, et al. Muraymycins, novel peptidoglycan biosynthesis inhibitors: synthesis and SAR of their analogues. Bioorganic & medicinal chemistry letters. 2003; 13:3345–3350. [PubMed: 12951123]
19. Lloyd AJ, Brandish PE, Gilbey AM, Bugg TD. Phospho-N-acetyl-muramyl pentapeptide translocase from Escherichia coli: catalytic role of conserved aspartic acid residues. Journal of bacteriology. 2004; 186:1747–1757. [PubMed: 14996806]
20. Mengin-Lecreulx D, Flouret B, van Heijenoort J. Cytoplasmic steps of peptidoglycan synthesis in Escherichia coli. Journal of bacteriology. 1982; 151:1109–1117. [PubMed: 6125497]
21. Chung BC, et al. Crystal structure of MraY, an essential membrane enzyme for bacterial cell wall synthesis. Science. 2013; 341:1012–1016. doi:10.1126/science.1236501. [PubMed: 23990562]
22. Al-Dabbagh B, et al. Active site mapping of MraY, a member of the polyprenyl-phosphate N-acetylhexosamine 1-phosphate transferase superfamily, catalyzing the first membrane step of peptidoglycan biosynthesis. Biochemistry. 2008; 47:8919–8928. doi:10.1021/bi8006274. [PubMed: 18672909]
23. Price NP, Momany FA. Modeling bacterial UDP-HexNAc: polyprenol-P HexNAc-1-P transferases. Glycobiology. 2005; 15:29R–42R. doi:10.1093/glycob/cwi065.
24. Izumi M, Yuasa H, Hashimoto H. Bisubstrate analogues as glycosyltransferase inhibitors. Current topics in medicinal chemistry. 2009; 9:87–105. [PubMed: 19199998]
25. Wang R, et al. A search for pyrophosphate mimics for the development of substrates and inhibitors of glycosyltransferases. Bioorganic & medicinal chemistry. 1997; 5:661–672. [PubMed: 9158864]
26. Gloster TM, Vocadlo DJ. Developing inhibitors of glycan processing enzymes as tools for enabling glycobiology. Nature chemical biology. 2012; 8:683–694. doi:10.1038/nchembio.1029. [PubMed: 22810773]
27. Rillahan CD, Brown SJ, Register AC, Rosen H, Paulson JC. High- throughput screening for inhibitors of sialyl- and fucosyltransferases. Angewandte Chemie. 2011; 50:12534–12537. doi:10.1002/anie.201105065. [PubMed: 22095645]
28. Rodolis MT, et al. Mechanism of action of the uridyl peptide antibiotics: an unexpected link to a protein-protein interaction site in translocase MraY. Chemical communications. 2014; 50:13023–13025. doi:10.1039/c4cc06516f. [PubMed: 25222373]
29. Dini C, et al. Synthesis of the nucleoside moiety of liposidomycins: elucidation of the pharmacophore of this family of MraY inhibitors. Bioorganic & medicinal chemistry letters. 2000; 10:1839–1843. [PubMed: 10969981]
30. Ii K, Ichikawa S, Al-Dabbagh B, Bouhss A, Matsuda A. Function-Oriented Synthesis of Simplified Caprazamycins: Discovery of Oxazolidine-Containing Uridine Derivatives as Antibacterial Agents against Drug-Resistant Bacteria. Journal of medicinal chemistry. 2010; 53:3793–3813. doi:Doi 10.1021/Jm100243n. [PubMed: 20405928]

References for methods

31. McCoy AJ, et al. Phaser crystallographic software. J Appl Crystallogr. 2007; 40:658–674. doi:10.1107/S0021889807021206. [PubMed: 19461840]

32. Adams PD, et al. PHENIX: a comprehensive Python-based system for macromolecular structure solution. Acta Crystallogr D Biol Crystallogr. 2010; 66:213–221. doi:S0907444909052925. [PubMed: 20124702]

33. Emsley P, Cowtan K. Coot: model-building tools for molecular graphics. Acta Crystallogr D Biol Crystallogr. 2004; 60:2126–2132. [PubMed: 15572765]

34. Clarke TB, et al. Mutational analysis of the substrate specificity of Escherichia coli penicillin binding protein 4. Biochemistry. 2009; 48:2675–2683. [PubMed: 19209901]

35. Dini C, et al. Synthesis of sub-micromolar inhibitors of MraY by exploring the region originally occupied by the diazepanone ring in the liposidomycin structure. Bioorganic & medicinal chemistry letters. 2002; 12:1209–1213. [PubMed: 11934590]

36. Hirano S, Ichikawa S, Matsuda A. Total synthesis of caprazol, a core structure of the caprazamycin antituberculosis antibiotics. Angewandte Chemie. 2005; 44:1854–1856. doi:10.1002/anie.200462439. [PubMed: 15723431]

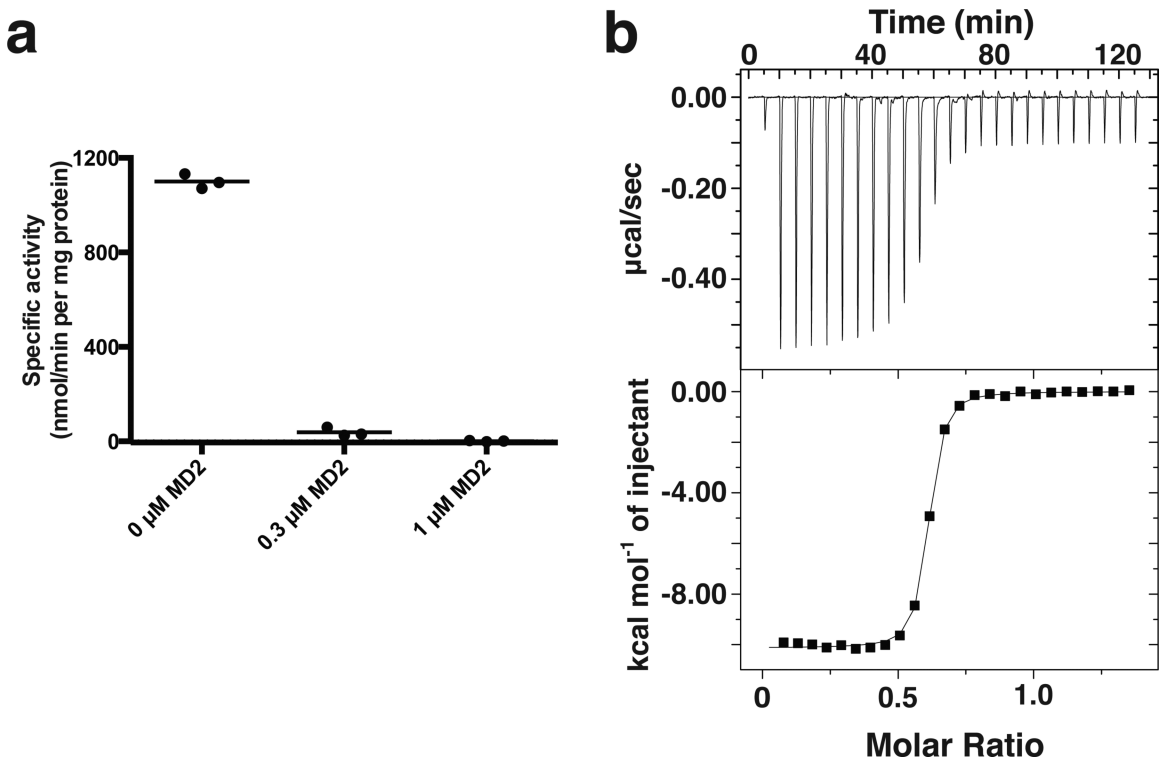

Figure 1. The natural product muraymycin D2 (MD2) binds to and inhibits $MraY_{AA}$

a, Specific activity measurements of $MraY_{AA}$ WT in the presence and absence of MD2 using radiolabeled substrate, [^{14}C]UM5A. The radiolabeled product, [^{14}C]Lipid I, was quantified using a liquid scintillation counting method (dpm). Three technical replicates are shown with the mean value indicated by a line. **b**, Representative ITC raw data and binding isotherm for MD2 interacting with $MraY_{AA}$ WT in the presence of 10 mM $MgCl_2$; K_D = 17.2 nM, $\Delta H° = -10.1$ kcal/mol. This ITC experiment was performed in triplicate (technical replicates) and mean thermodynamic parameters are shown in Extended Data Table 2.

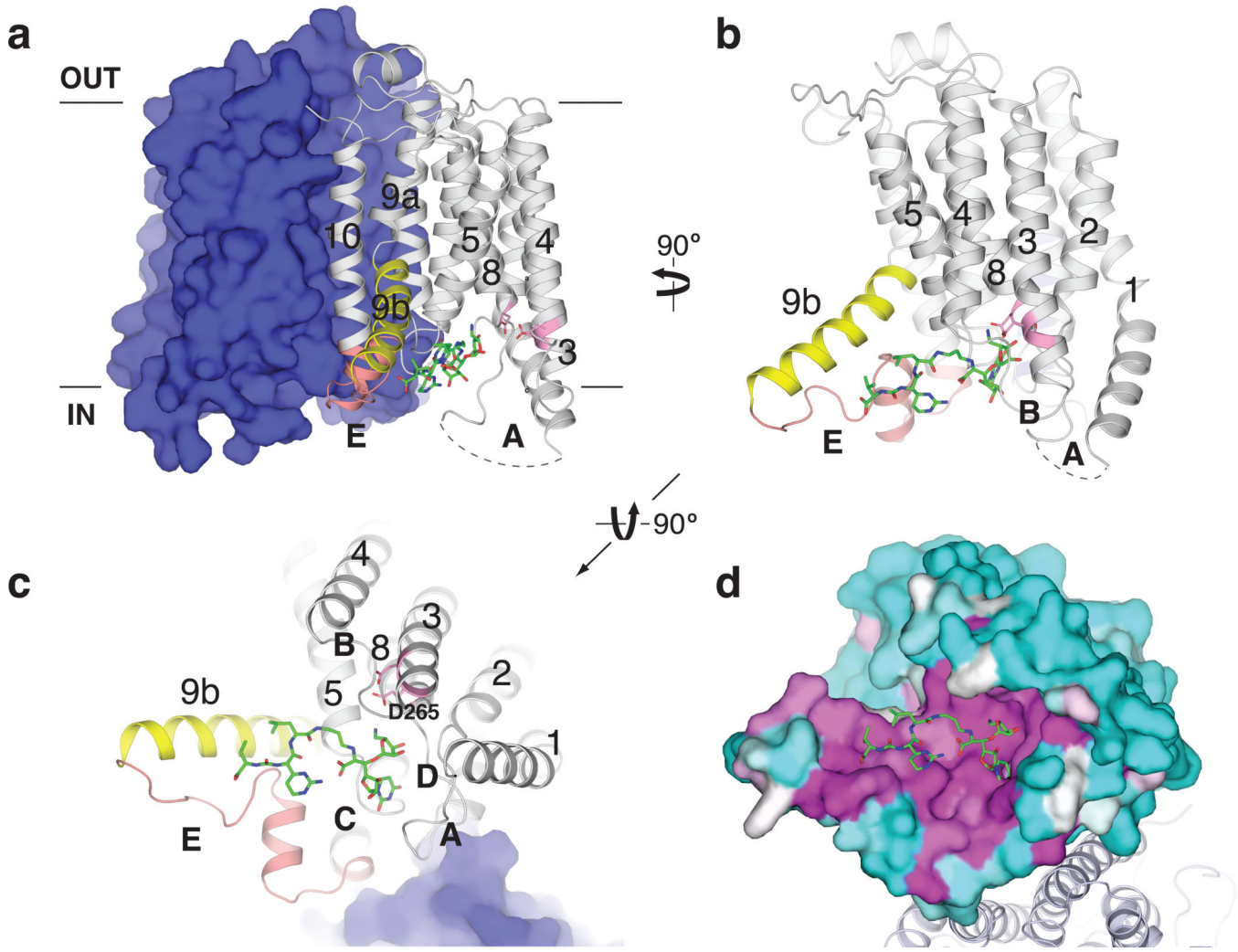

Figure 2. MD2 binds to a conserved site in MraY$_{AA}$

a, The MD2-bound MraY$_{AA}$ dimer viewed from the membrane. One protomer is shown as surface representation and the other as a cartoon. MD2 (green sticks) resides in the pocket formed by TMs 3-5 and 8-9b and cytoplasmic loops B-E. Conserved catalytic aspartic acid residues at the active site are shown in pink. **b,** View from the membrane rotated 90° about a vertical axis relative to (**a**). One protomer is shown for clarity. **c,** Cytosolic view of the MraY$_{AA}$-MD2 complex, rotated 90° about a horizontal axis relative to (**b**). Part of MD2 is near the putative substrate recognition site formed by TM9b (yellow) and loop E (orange). **d,** Conservation mapping of MraY$_{AA}$ from high (magenta) to low (cyan) sequence identity, based on the alignment of 28 MraY homologs [21].

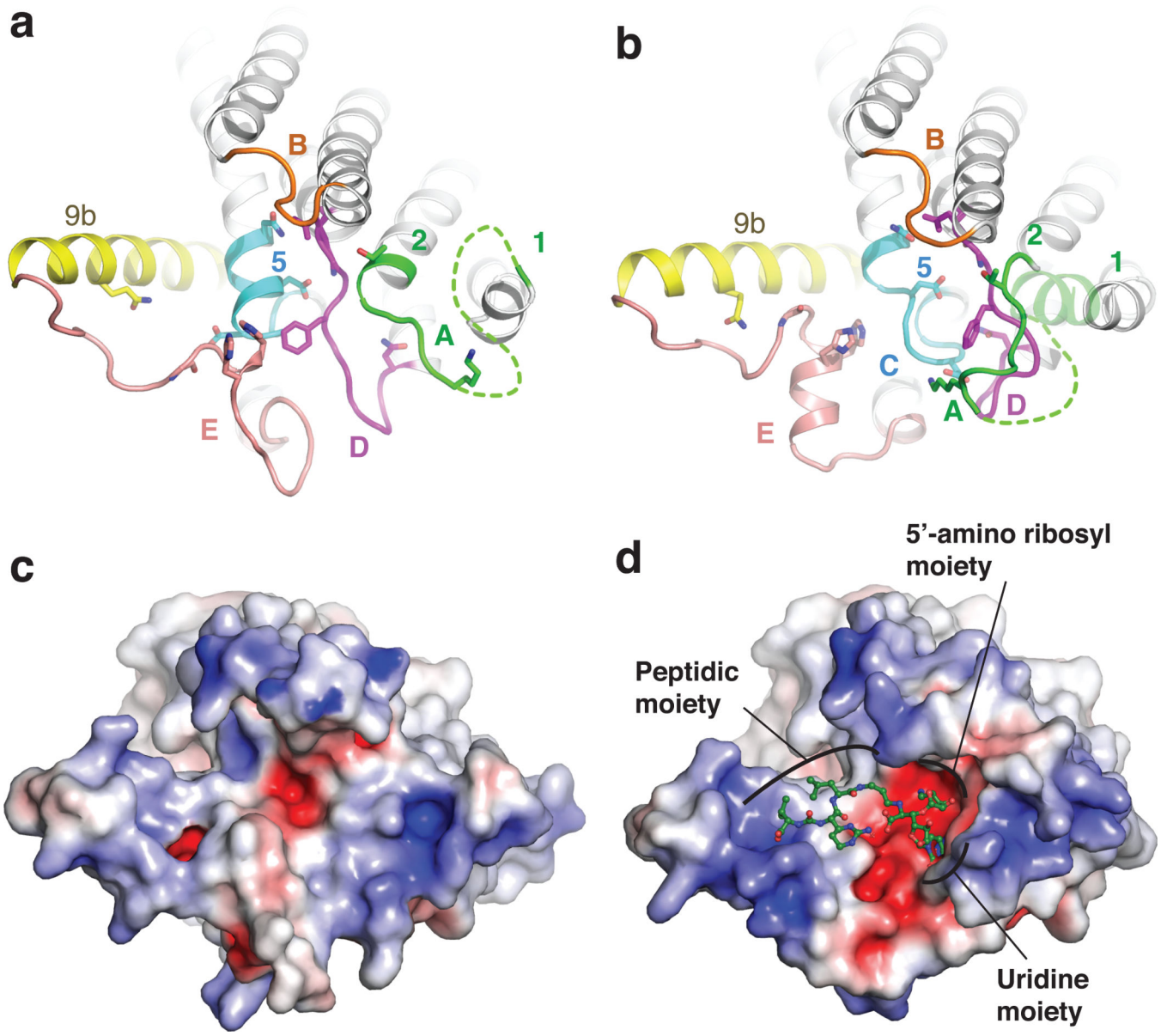

Figure 3. Conformational rearrangement of MraY$_{AA}$ upon MD2 binding

a, apoMraY$_{AA}$ (PDB ID: 4J72) viewed from the cytoplasm, as in Fig. 2c. Residues involved in interactions with MD2 are shown as sticks. **b,** MD2-bound MraY$_{AA}$ with MD2 omitted. Part of TM1 (light green) is transparent due to its absence in the apoMraY$_{AA}$ structure. **c,** Electrostatic surface representation of apoMraY$_{AA,}$ viewed from the cytoplasm as in a-b. **d,** Electrostatic surface representation of MraY$_{AA}$ in complex with MD2. MD2 is green and shown in ball-and-stick representation.

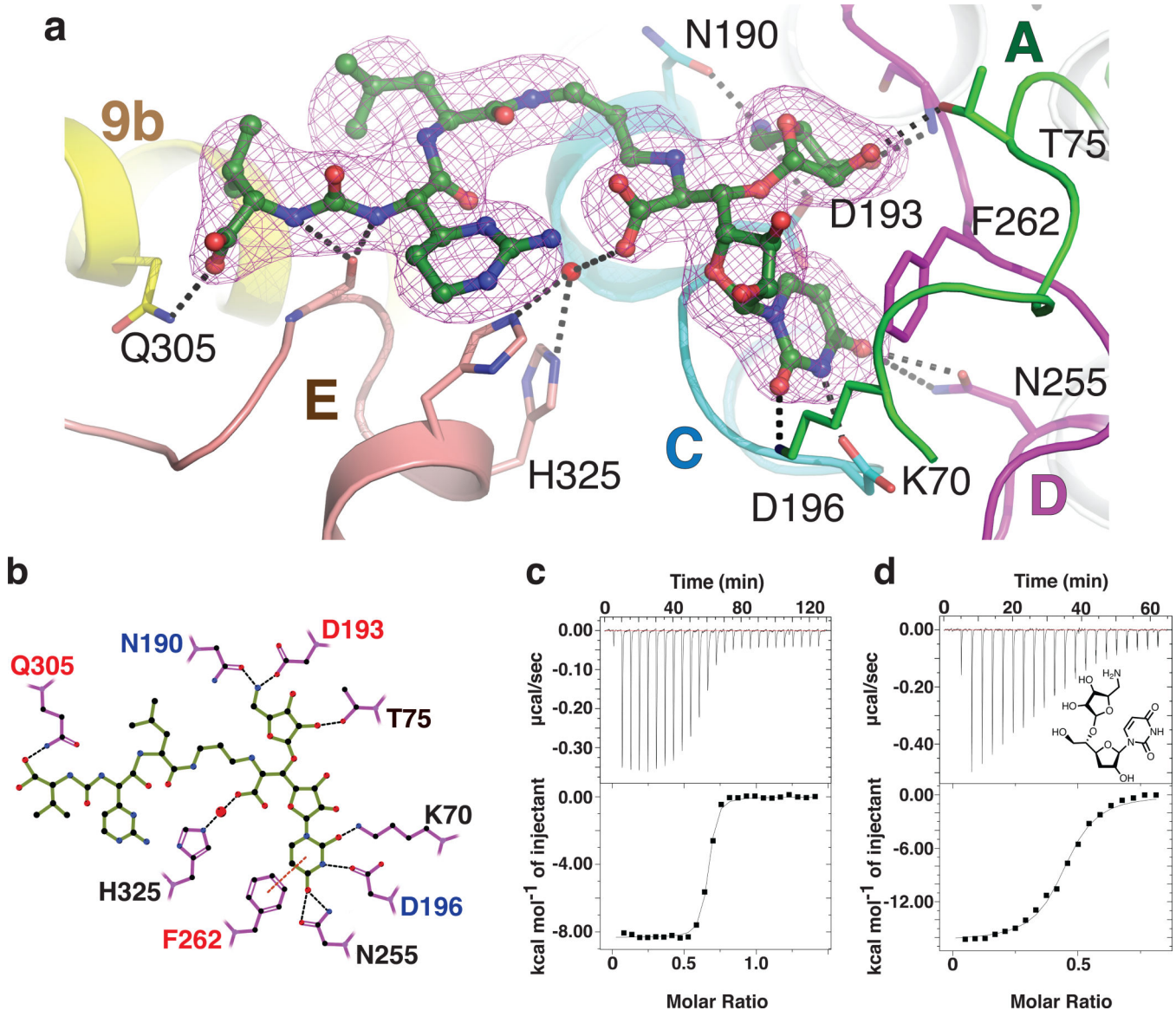

Figure 4. Dissection of the interactions between MD2 and MraY$_{AA}$ elucidates the chemical logic of MraY$_{AA}$ inhibition

a, Composite simulated annealing $2F_o–F_c$ omit electron density of MD2 in the crystal structure of MD2-bound MraY$_{AA}$ at 1.7σ. The TMs are colored as in Fig. 3, a-b. The residues forming side chain interactions with MD2 are labeled. **b**, A two-dimensional representation of the interactions between MD2 and MraY$_{AA}$. Hydrogen bonds (3.2 Å cutoff) are indicated with black dashed lines and $\pi–\pi$ contacts are indicated with red dashes. Mutation of residues with red colored labels resulted in a larger than five-fold increase in the K_D of MD2 and those with blue residue labels are nearly inactive. **c**, Representative ITC raw data and binding isotherm for MD2 titrated into MraY$_{AA}$ in the absence of added Mg^{2+}; K_D = 14.8 nM, ΔH° = −8.3 kcal/mol. A similar K_D is observed for MD2 titrated into MraY$_{AA}$ with added Mg^{2+}. **d**, Representative ITC raw data and binding isotherm for 5-aminoribosyl-3-deoxy uridine titrated into MraY$_{AA}$ WT; K_D = 283 nM, ΔH° = −16.4 kcal/

mol. Each ITC experiment was performed in triplicate (technical replicates) and mean thermodynamic parameters are shown in Extended Data Table 2.